https://doi.org/10.26599/FRICT.2026.9441268

Research Article

A state-conditioned recognition framework for TBM cutter using mechanism-guided historical statistics and deep observations

Jiliang Mo[1,2], Shengxin Wang[1,2], Zhiyao Zhang[1,2], Tixiang Xiong[1,2], Mengqi Zhang[1,2,*]

[1] Institute of Tribology, School of Mechanical Engineering, Southwest Jiaotong University, Chengdu 610031, China

[2] Tribological Design Laboratory for Shield/TBM Equipment, Southwest Jiaotong University, Chengdu 610031, China

[*] Corresponding author: Mengqi Zhang (mzhang@swjtu.edu.cn)

Received: March 8, 2026; Revised: May 2, 2026; Accepted: May 20, 2026

© The Author(s) 2026.

Just Accepted

Abstract

This study tackles reliable recognition of TBM cutter damage state under complex and varying operating conditions, where vibration responses are broadband, strongly non-stationary, and dominated by randomly excited impacts, making stable fault characteristic frequencies difficult to extract. Using a scaled multi-cutter rock-breaking bench platform, we show that partial wear induces a fundamental transition in cutter-rock contact from rolling indentation to sliding scraping, thereby reshaping the energy distribution and impact-related statistics. Guided by this mechanism, we design physically interpretable state proxies to represent history-accumulated statistical signatures of damage. We further propose a mechanism-guided state-conditioned recognition framework that decouples instantaneous observations from historical-state information: a deep observation encoder (DCNN or Transformer) learns window-level dynamic-response features from raw multi-channel vibration segments, while a mechanism-guided state

estimator computes state proxies from historical statistics and uses them as a state-conditioned constraint for decision making. To align offline learning with online monitoring, the estimator employs global statistics during training to establish stable reference baselines, but switches to historical statistics during testing to avoid future-information leakage. Cross-condition evaluations demonstrate improved robustness to distribution shifts, achieving peak accuracies of 92.17% (DCNN) and 88.91% (Transformer), with time-evolution results indicating progressive stabilization as historical statistics accumulate. Ablation results verify the complementary contributions of different proxies and show a marked drop when state variables are removed (down to 64.73%), confirming that performance gains stem from state-conditioned constraints rather than increased model complexity. Overall, the proposed framework provides an interpretable and practically oriented route toward more stable cutter-state monitoring under varying operating conditions.

Keywords: TBM cutter; Partial wear; Vibration analysis; State recognition; Tribology; Deep learning

Just Accepted

1. Introduction

Tunnel Boring Machines (TBMs), as the core equipment for complex underground construction, play a decisive role in construction safety, operational efficiency, and economic cost control[1, 2]. During TBM excavation, the cutter, serving as the key execution component directly involved in rock fragmentation, endures intense impact loads, high-frequency vibrations, and complex geological coupling effects over extended periods. The degradation and abnormal wear of cutters are among the primary factors leading to reduced excavation efficiency, equipment damage, and even unplanned downtime[3-7]. Therefore, accurate state recognition and continuous monitoring of cutters are of critical engineering significance for ensuring the safe and stable operation of TBMs[3, 8, 9].

Compared with indirect monitoring indicators such as temperature, current, or thrust parameters, vibration signals directly reflect the dynamic interaction characteristics of the cutter-rock contact process and are regarded as one of the most sensitive data sources for characterizing cutter working states[5, 8, 10]. From a tribological perspective, the cutter-rock interaction can be viewed as a complex frictional interface evolution process involving contact-mode transitions, energy dissipation, and surface response variations under varying loading conditions[11-14]. However, the TBM construction environment exhibits strong non-stationarity and pronounced working-condition coupling. Variations in geological conditions, operational parameters, and multi-cutter cooperative interactions can induce substantial fluctuations in vibration responses, posing significant challenges to robust cutter state recognition[9, 15-17]. Consequently, there is an urgent need for a state recognition method that operates reliably under complex operating conditions while maintaining strong generalization capability and interpretability.

Existing cutter state recognition methods can generally be categorized into two groups. The first group relies on manually designed time-domain or frequency-domain statistical features

combined with shallow machine learning models such as Support Vector Machines (SVM) and Random Forests (RF) for state classification[8, 18-20]. For instance, Li et al. conducted online state monitoring of key TBM components by decomposing vibration signals and extracting statistical features, followed by SVM-based classification, thereby demonstrating the feasibility of the "feature engineering + SVM" paradigm for non-stationary vibration data in engineering equipment[18]. Akhlaghi et al. further incorporated multidimensional handcrafted time-frequency features derived from both acoustic and vibration signals, comparing decision trees and RF for cutter wear prediction, and showed that tree-based ensemble learning can effectively characterize wear under complex operating conditions[8]. Mahmoodzadeh et al. constructed feature vectors using field-collected TBM operational parameters and geological information, and employed Support Vector Regression (SVR) models to predict cutter life, providing data-driven support for cutter replacement decision-making [19]. In addition, Zhou et al. addressed fault diagnosis for dual-shield TBMs using SVM-based classification boundary construction, confirming that SVM-type shallow models still retain certain engineering applicability in equipment state recognition tasks[20]. Although these methods exhibit a degree of physical interpretability, their performance heavily depends on feature engineering experience and is limited in representing complex non-stationary vibration signals. Under varying operating conditions or cross-scenario applications, their recognition accuracy often deteriorates significantly, making them insufficient for practical engineering deployment.

With the rapid advancement of deep learning, data-driven models such as Convolutional Neural Networks (CNNs) and Transformer architectures have been increasingly applied to machinery state recognition tasks. Chen et al. transformed raw vibration signals into time-frequency maps using Continuous Wavelet Transform (CWT) and developed a CNN-ELM diagnostic framework, achieving higher classification accuracy with reduced computational cost on gearbox and bearing datasets[21]. Liu et al. applied CNN models including GoogLeNet and ResNet to time-frequency representations of TBM vibration signals, enabling geological face recognition during excavation and demonstrating the applicability of deep models to certain tunneling conditions[15]. Li et al. proposed a Transformer-based meta-learning framework (ETML) that rapidly adapts to new operating conditions in small-sample bearing fault scenarios while maintaining high recognition performance[22]. Xiang et al. further introduced frequency-domain channel attention into a Vision Transformer framework to highlight critical frequency components, improving robustness under cross-condition bearing fault identification and providing interpretability through attention visualization[23]. These approaches are capable of learning high-dimensional representations directly from raw vibration data and often achieve superior accuracy on specific datasets. However, purely data-driven models typically lack physical constraints and are prone to learning spurious condition-dependent features, resulting in strong reliance on the training data distribution[24, 25]. When discrepancies exist between training data and real engineering environments, their recognition accuracy tends to fluctuate significantly[26-28]. Furthermore, such methods typically perform classification based on a single time window, neglecting the cumulative patterns induced by changes

Just Accepted

in equipment states. Consequently, the model essentially relies on ‘instantaneous responses’ to infer ‘long-term states’, which becomes an important factor leading to insufficient cross-condition generalization capability[24, 29].

In practice, cutter wear is a gradually accumulated background condition, whereas a single vibration window only reflects the cutter’s dynamic response under a specific instantaneous operating condition. Due to continuously varying cutter-rock contact conditions during excavation, similar instantaneous vibration responses may correspond to entirely different cutter wear states. Consequently, models relying solely on instantaneous signals are highly susceptible to misinterpreting working-condition variations as state transitions. Therefore, the core challenge of TBM cutter state recognition lies in effectively associating short-term vibration responses with long-term state information under complex and varying operating conditions.

To address this challenge, this study proposes a TBM cutter state recognition framework that integrates vibration-mechanism based statistical features with deep learning models. From an information-structural perspective, the proposed approach reconstructs the state recognition process. The deep learning module is responsible for analyzing local impact characteristics and waveform patterns within the current vibration window to capture the cutter’s instantaneous response behavior. Meanwhile, statistical features derived from vibration mechanisms are introduced to characterize the evolutionary trends of vibration energy and response levels over historical time scales, thereby capturing the cumulative characteristics of the cutter damage state. In the decision-making process, the model no longer relies solely on isolated instantaneous observations, but instead evaluates the current vibration under the combined context of known damage states and historical operating conditions, thereby effectively reducing the risk of misclassification caused by variations in operating conditions.

To ensure consistency between model training and practical online monitoring environments, a differentiated mechanism-feature construction strategy is further developed for the training and testing phases. During model training, complete sequences are utilized to establish stable statistical reference baselines for state representation, thereby enhancing the stability of decision boundary learning. In contrast, during testing and real-world deployment, only historical data prior to the current time are used for statistical estimation, preventing information leakage from future data and ensuring practical implementability. This design guarantees causal consistency between offline training and online application, thereby avoiding discrepancies between experimental performance and field deployment outcomes.

Based on multi-cutter rock-breaking test data, mechanism-based statistical features are constructed from both vibration mechanisms and cutterhead spatial configurations. These features are fused with deep learning representations through a simple yet effective concatenation strategy. The proposed method exhibits the following advantages: (1) By separately modeling instantaneous responses and cumulative states, cross-condition recognition robustness is significantly improved. (2) Mechanism-guided state variables (used as state proxies) reflect long-term evolution, enhancing

Just Accepted

physical interpretability. (3) The historical state estimation mechanism is designed to be consistent with the requirements of real-time engineering monitoring, facilitating the transition from laboratory validation toward practical deployment. (4) The strategy operates at the feature representation level and can be flexibly integrated with various deep learning backbones, demonstrating strong architectural generality. Experimental results demonstrate that the proposed method effectively improves the recognition stability under cross-operating conditions. Furthermore, time-evolution analysis and ablation experiments were conducted to validate the model performance. The results not only confirm the effectiveness of the proposed approach but also quantitatively evaluate the contributions of different mechanism-based features to the recognition performance.

The main contributions of this study are summarized as follows:

1. Multi-condition multi-cutter cooperative rock-breaking tests are conducted, and physically meaningful and robust state representation features are identified through vibration mechanism analysis.

2. A differentiated mechanism-feature construction strategy for training and testing phases is proposed. During training, complete data are used to establish reference baselines for mechanism-based statistical features; during testing and deployment, only historical data prior to the current time are used for statistical estimation, satisfying the practical constraints of online monitoring scenarios encountered in engineering applications.

3. A state-conditioned recognition framework for TBM cutter is developed. Through a simple yet effective feature concatenation strategy, long-term background information and instantaneous vibration responses are jointly represented, enhancing both the interpretability and cross-model generalization capability of the proposed method.

4. The effectiveness of the proposed method is validated on two representative deep learning models. Through accuracy-time curve analysis and ablation studies, the method further quantifies the temporal evolution of performance and evaluates the contributions of different mechanism-based features to the recognition results.

The remainder of this paper is organized as follows. Section 2 introduces the test bench setup. Section 3 presents mechanism analysis based on bench test results. Section 4 describes the proposed state recognition method in detail. Section 5 provides experimental settings and result analysis. Finally, Section 6 concludes the paper and discusses future research directions.

2. Bench Test Setup

Partial wear is a typical abnormal damage state of TBM cutters, characterized by localized material loss occurring only in specific regions of the cutter ring rather than uniformly along the entire circumference. This phenomenon usually occurs when the cutter cannot rotate freely during the rock-breaking process, often due to bearing jamming or rotation obstruction. As a result, the cutter ring experiences sliding contact with the rock instead of normal rolling, leading to

Just Accepted

concentrated wear in limited areas while other parts remain relatively intact. Consequently, the originally circular cutter ring gradually develops a flattened wear zone and becomes geometrically asymmetric. A comparison between a normal cutter and a cutter with partial wear is shown in Fig. 1. To investigate the vibration characteristics associated with this wear state, rock-breaking bench tests were conducted as described in the following section.



Fig. 1 Comparison of typical normal and partially worn cutters

2.1 Test Conditions

(1) Test bench system: A self-designed scaled TBM cutter rock-breaking test platform was employed in this study, consisting of a hydraulic system, motor drive system, control system, cutterhead, and rock specimen assembly, as illustrated in Fig. 2[30]. During testing, the hydraulic system drives the cutterhead toward the rock surface, enabling the cutters mounted on the cutterhead to penetrate the rock and simulate the indentation process. Meanwhile, the motor system rotates the rock specimen about a central axis shared with the cutterhead, generating relative rotational motion between the cutters and the rock. The combination of cutter penetration toward the rock face and rotational motion of the rock specimen reproduces the complete rock-breaking process. For data acquisition, the test platform was equipped with high-precision sensors, including four tri-axial force sensors and two tri-axial accelerometers. The force sensors were installed between the cutter seat and the cutterhead, enabling accurate measurement of cutter loads during rock breaking. The tri-axial accelerometers were mounted on the side surface of the cutter seat to directly capture vibration signals generated during the cutter-rock interaction. The sampling frequency was set to 1 kHz for force sensors and 5 kHz for acceleration sensors.

(2) Test cutters: Scaled disc cutters with an outer diameter of 86 mm were used in the tests, corresponding to an approximate geometric scaling ratio of 1:5 relative to full-scale TBM cutters. The structural configuration of the scaled cutter is consistent with that of a full-scale cutter, comprising a cutter ring, cutter shaft, bearings, and associated components. The cutter seat was designed as a detachable structure and could be mounted at different positions on the cutterhead to facilitate cutter replacement and adjustment of cutter spacing during testing. The cutter material was H13 tool steel. The heat treatment procedure involved three-stage heating at 650 °C, 850 °C, and 1020 °C, respectively, each held for 2-3 hours, followed by quenching. After the cutter ring cooled to room temperature, two tempering treatments were conducted at 550 °C for 4-5 hours each to relieve residual stresses induced during quenching. After heat treatment, the average surface hardness of the cutter ring reached 58 HRC. To simulate partial wear conditions, a partial wear depth

Just Accepted

of 2 mm was pre-machined on one side of the scaled disc cutter, and the detailed geometry is illustrated in Fig. 3.

(3) Rock specimens: Natural granite was selected for the rock-breaking tests. Rock blocks without visible macro-cracks were cut and processed into specimens with flat surfaces to ensure proper contact between the cutter and the rock. The specimen dimensions were 1000 mm × 1000 mm × 120 mm. Each rock specimen was fixed within a steel container using concrete to prevent displacement during testing. The macroscopic mechanical properties of the rock were characterized according to the Chinese standard GB/T 50266-2013 Standard for Test Methods of Engineering Rock Masses. The measured mechanical parameters were as follows: Young's modulus 20.36 GPa, Poisson's ratio 0.177, uniaxial compressive strength 111.75 MPa, and tensile strength 5.03 MPa.

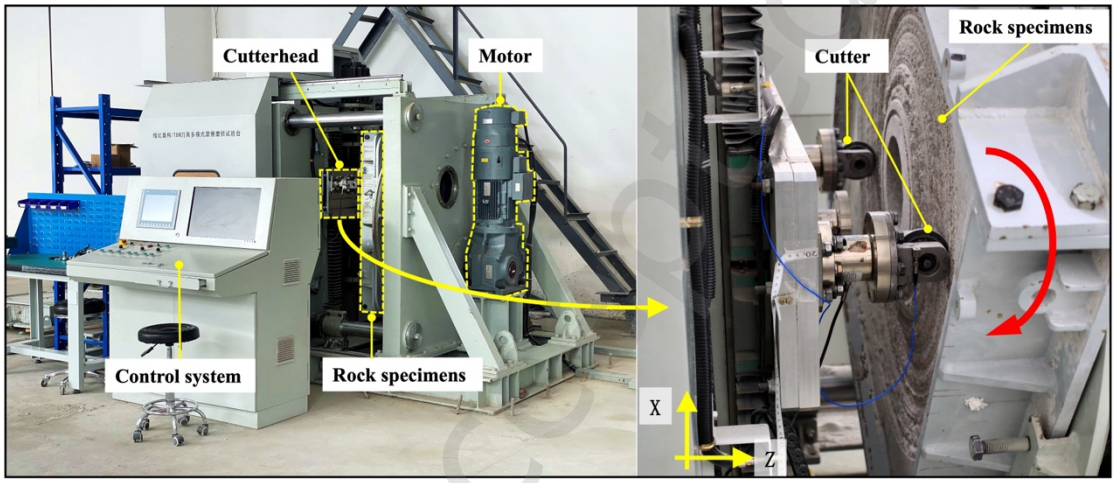


Fig. 2 Scaled TBM cutter rock-breaking test platform

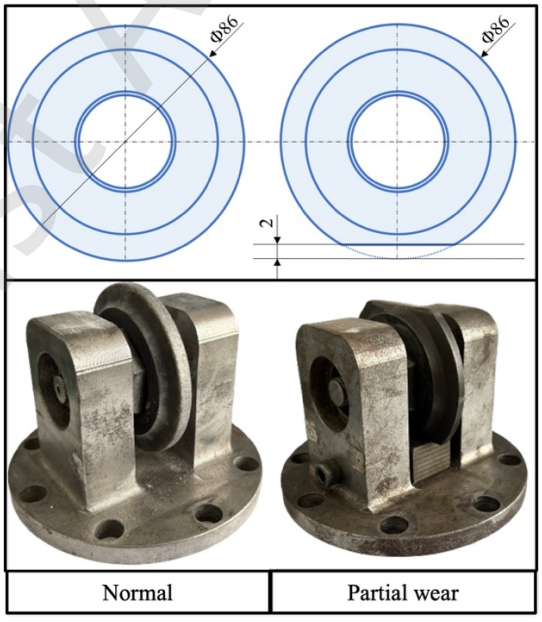


Fig. 3 Detailed geometry and dimensions of normal and partial worn cutters

2.2 Test Scheme

To validate the generalization capability and engineering applicability of the proposed cutter state recognition method under complex varying operating conditions, multiple combinations of

thrust and rotational speed were designed. In practical engineering scenarios, complex geological variations (e.g., abrupt changes in rock strength) and fluctuations in excavation parameters (e.g., cutter penetration depth) are ultimately reflected in variations of the total cutterhead thrust. Therefore, total cutterhead thrust was selected as the primary macroscopic indicator representing the overall cutter loading level. In addition, as modern TBMs continue to increase in excavation diameter, cutters installed in the outer radial region of the cutterhead operate at significantly higher linear velocities than central cutters. The substantial increase in linear velocity directly alters the kinetic energy and impact dynamics during rock breaking, leading to pronounced differences in system vibration responses. Therefore, cutter rotational speed (and thus linear velocity) must also be considered in the test design. Based on these engineering considerations, three representative combinations of thrust and rotational speed were selected: (1) Load A: F=5 kN， ω=1 r/min；(2) Load B: F=10 kN，ω=1 r/min；(3) Load C：F=5 kN，ω=0.5 r/min. These three operating conditions cover the fundamental variation ranges of the two key influencing factors, namely rotational speed and load, encompassing combinations of low/high speed and low/high load. Among them, Load A can be regarded as the baseline condition, Load B primarily reflects the effect of load variation, and Load C is designed to characterize the influence of rotational speed variation on vibration response characteristics.

On the other hand, considering that high-frequency vibration signals experience significant path attenuation when propagating through complex mechanical structures, the relative spatial position between sensors and damaged cutters plays a decisive role in extracting weak fault features. As shown in Fig. 4, six cutters were installed on the test cutterhead to simulate the cooperative rock-breaking behavior of multiple cutters. The spacing between adjacent cutters was set to 25 mm, and the installation radius of the innermost central cutter was 155 mm. To comprehensively evaluate spatial attenuation effects, two key acceleration measurement points were configured: Sensor 1 was directly mounted on the cutter seat of the upper left cutter to capture source-level vibration signals of an individual cutter. Sensor 2 was installed on the main panel of the cutterhead to monitor system-level coupled vibrations induced by multi-cutter rock breaking. Three different cutter health-state and spatial-distribution scenarios were designed: Healthy state: (1) All cutters were undamaged. This configuration served as the baseline condition for subsequent testing. (2) Partial wear - upper right position: The partially worn cutter was installed at the upper right inner position (yellow marker in Fig. 2) with an installation radius of 180 mm. In this case, the damaged cutter was not co-located with either sensor. (3) Partial wear - upper left position: The partially worn cutter was installed at the upper left position with an installation radius of 205 mm, corresponding to the location of Sensor 1. In this scenario, the damaged cutter was closest to the vibration measurement point. In summary, the test matrix comprised 3 loading conditions and 3 cutter spatial-damage configurations. By fully crossing these factors, a total of 9 independent rock-breaking test conditions were conducted.

Just Accepted

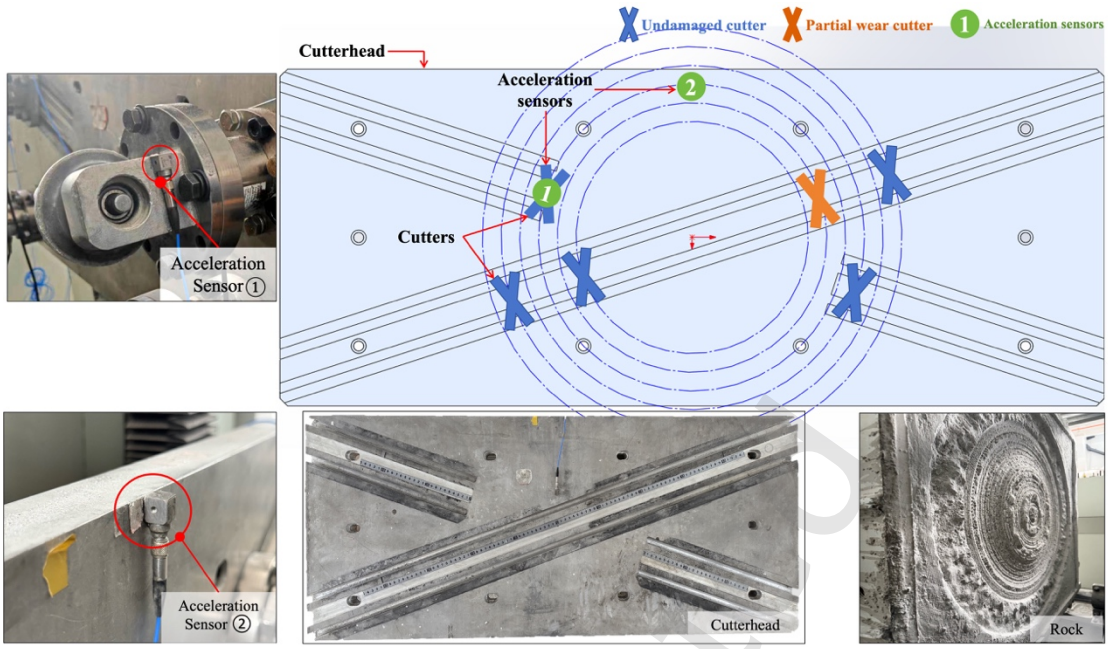


Fig. 4 Illustration of the bench test setup

3. Test Results and Mechanism Analysis

The raw acceleration signals acquired during the tests are shown in Fig. 5. The data were collected from Sensor 2 mounted on the cutterhead, and the test group in which the partially worn cutter was positioned at the upper right location is presented as a representative example. As illustrated in Fig. 5, under all operating conditions, the cutter vibration signal consists of multiple discrete impact events. The occurrence time, frequency, and amplitude of these impacts exhibit no apparent deterministic pattern, suggesting that the vibration response of the cutter is predominantly governed by randomly induced impact excitations. This vibration characteristic corresponds closely to the rock-breaking mechanism of disc cutters. Under compressive loading from the cutter, the rock undergoes discontinuous brittle fracture. At the instant of fracture, the strain energy stored within the rock is suddenly released, generating an impact excitation that triggers system vibration. However, due to material heterogeneity within the rock mass and macroscopic surface irregularities, the occurrence of brittle fracture is inherently stochastic in both intensity and frequency. Consequently, the resulting vibration response exhibits strong randomness[31].

Just Accepted

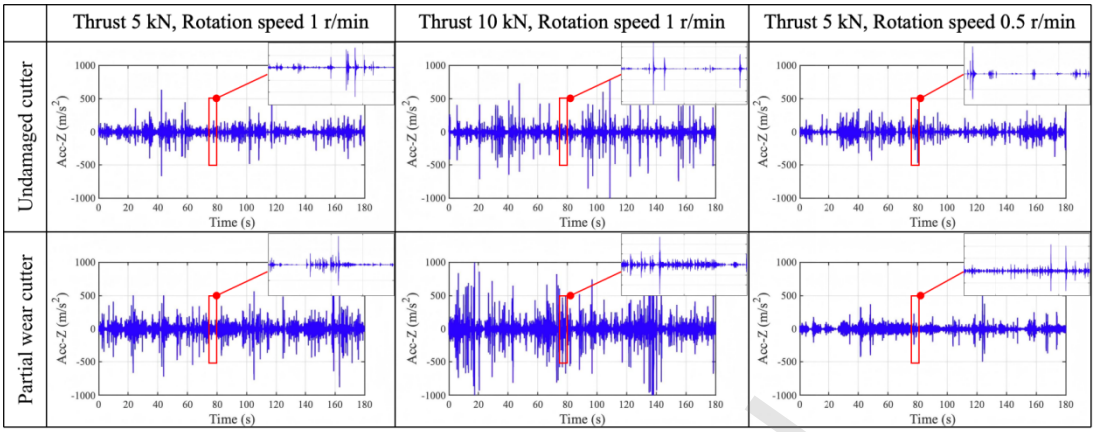


Fig. 5 Raw normal acceleration signals of the cutter

Fig. 6 presents the envelope spectra of vibration signals for normal cutters and partially worn cutters under different thrust and rotational speed conditions. From the frequency-domain responses, it can be observed that regardless of cutter health state or operating condition, the envelope spectra exhibit pronounced broadband stochastic characteristics. The energy is primarily concentrated in the low-frequency range and decays gradually with increasing frequency. No distinct discrete spectral lines associated with cutter rotational frequency or characteristic fault frequencies are observed. Even under partial wear conditions, although slight amplitude fluctuations can be identified in the low-frequency band, these remain submerged within the broadband noise background and do not form identifiable periodic impact peaks. This indicates that vibration generated during cutter rock-breaking is dominated by random rock-fracture impacts, resulting in highly non-stationary and weakly periodic signal characteristics.

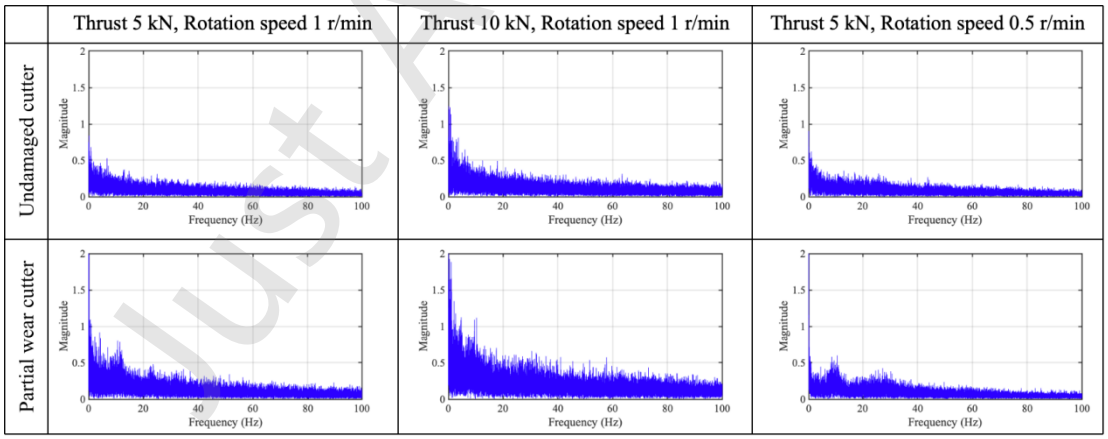


Fig. 6 Envelope FFT of cutter normal acceleration

To quantitatively evaluate the differences in vibration energy transmission between normal and partially worn cutters, the vertical acceleration root mean square (RMS) values were calculated at both the cutter-mounted sensor and the cutterhead-mounted sensor under different operating conditions. In addition, the RMS ratio between horizontal and vertical directions was computed. The statistical results are presented in Fig. 7 and Fig. 8, respectively. The results indicate that under identical operating conditions, once a cutter experiences partial wear, the acceleration RMS values increase significantly at both the cutter-mounted sensor and the cutterhead-mounted sensor

Just Accepted

compared with the normal state. The underlying physical mechanism is that partial wear prevents the cutter from rotating smoothly about its axis. As a result, the cutter-rock interaction mode transitions from rolling indentation to sliding scraping. This sliding contact substantially increases frictional resistance at the interface and may induce pronounced stick-slip effects and unstable tangential impacts during rock breaking, thereby injecting higher energy into the vibration system.

Load conditions generally exert a positive influence on vibration intensity. As shown in Fig. 7, in most cases, the high-thrust and high-speed combination (Case 2) corresponds to higher RMS values. However, the test data reveal that the relationship between vibration response and nominal load is not strictly linear but exhibits significant nonlinearity. Notably, when the upper left cutter experiences partial wear (Case 1 vs. Case 2), although Case 2 has a higher nominal load, the RMS value measured by Sensor 1 (21.5) is substantially lower than that of Case 1 (43.0). This apparent anomaly can be attributed to the non-uniform load distribution in multi-cutter cooperative rock-breaking systems. During multi-cutter interaction, the actual penetration depth of each cutter is influenced by installation tolerances and rock surface irregularities. Consequently, a partially worn cutter may experience passive unloading and bear a relatively low effective load, leading to weakened correlation between single-point vibration intensity and total cutterhead thrust.

Practical experience further indicates that acceleration RMS is strongly coupled with multiple factors, including total cutterhead thrust, rotational speed, rock strength, and cutter damage state, thereby lacking specificity as an independent diagnostic indicator. For example, under the high-load Case 2 condition, even normal cutters exhibit an RMS value (12.3) higher than that of partially worn cutters under the lower-load Case 3 condition (11.1). This implies that simple energy-threshold-based criteria are prone to false-negative misjudgments. In real engineering scenarios involving heterogeneous strata, fractured zones, or isolated boulders, geological variations often mask the subtle energy increments caused by a single damaged cutter. Therefore, RMS-based time-domain statistical analysis alone is insufficient for accurate early-stage fault recognition.

Just Accepted

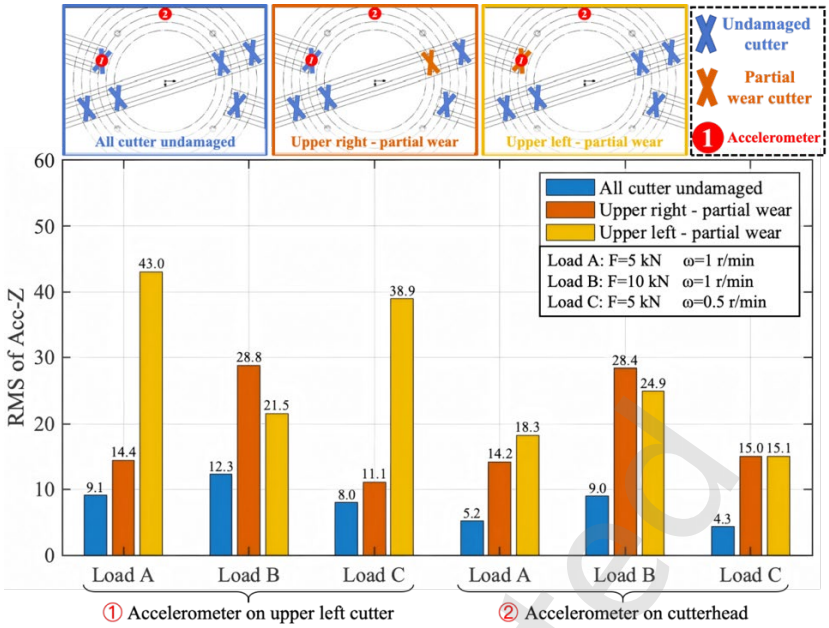


Fig. 7 RMS of normal acceleration

To further explore dimensionless indicators, the Cutting Coefficient (CC) is introduced, defined as the ratio between the RMS value of tangential acceleration (X-direction, corresponding to the feed direction) and the RMS value of normal acceleration (Z-direction, perpendicular to the rock surface). As shown in Fig. 8, for the normal cutter group, the CC value remains within a relatively narrow range regardless of load variations. Taking Sensor 1 as an example, under three significantly different load conditions, the CC values are 0.44, 0.42, and 0.40, respectively, with a maximum relative deviation of only 9.5%. This fluctuation is substantially smaller than the 34.5% sensitivity observed in acceleration RMS under the same conditions. The reason lies in the mechanical relationship during normal rolling rock breaking: the tangential cutting resistance and the normal penetration force follow a geometric decomposition relationship determined primarily by cutter geometry and rolling friction coefficient, and are only weakly correlated with total thrust or rotational speed. Consequently, under healthy rolling conditions, vibration energy in the X and Z directions maintains a stable proportional relationship.

However, once partial wear occurs, the CC response exhibits a dramatic reversal. As shown in Fig. 8, in all test cases involving partially worn cutters, CC values increase significantly compared to their normal counterparts. In particular, when the monitored cutter itself (upper left position) experiences partial wear (yellow bars), CC shows explosive growth. For example, under Load B, the CC value increases from 0.42 in the normal state to 2.78 under partial wear, corresponding to an increase exceeding 560%. This phenomenon arises because partial wear transforms cutter motion from rolling to sliding. According to tribological principles, the sliding friction coefficient of rock is substantially higher than the rolling friction coefficient, causing disproportionate growth in tangential resistance and vibration components. As a result, the original mechanical force balance is disrupted. Since CC is strongly associated with cutter motion mode and weakly dependent on working-condition variations, it demonstrates potential as an indicator for partial wear recognition.

Just Accepted

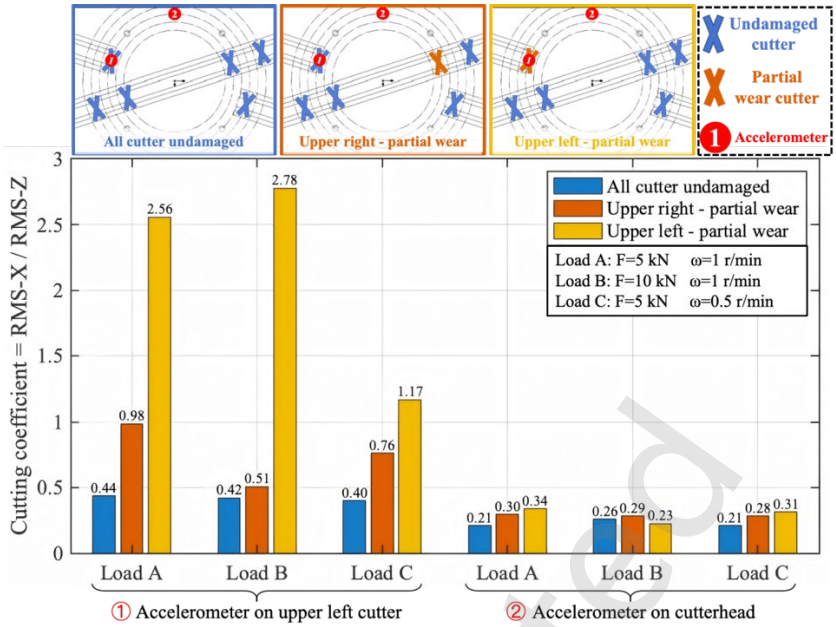


Fig. 8 Cutting coefficient

The kurtosis values of the Z-direction acceleration measured at the cutterhead central sensor are presented in Fig. 9. The results show that under all three load conditions (Load A, B, and C), the normal cutter group exhibits consistently high kurtosis values ranging from 79.2 to 88.2. In contrast, once partial wear exists within the system—regardless of whether it is located at the upper left or upper right position—the kurtosis values decrease significantly. For example, under Load B, the normal group shows a kurtosis value of 88.19, while the upper right and upper left partially worn groups decrease to 46.50 and 28.11, corresponding to reductions of 47.3% and 68.1%, respectively. The reduction in kurtosis is also fundamentally linked to the transition from rolling indentation to sliding scraping. Specifically: (1) Normal state: Rock breaking occurs in discrete intermittent bursts. The cutter ring rolls along the rock surface, accumulates stress, and suddenly fractures the rock, followed by unloading. This process generates sparse high-amplitude impact peaks superimposed on a low-amplitude background, resulting in a long-tailed probability distribution and extremely high kurtosis values. (2) Partial wear state: Continuous sliding friction and scraping introduce dense broadband random vibration into the system. This fills the low-amplitude intervals in the signal, making the amplitude distribution more Gaussian-like and flattening the probability density function, ultimately leading to significantly reduced kurtosis. Although load variations (Load A/B/C) induce certain fluctuations in kurtosis values, a clear separation remains between the baseline normal state (~80) and the partially worn state (<50). This demonstrates that kurtosis is highly sensitive to changes in cutter motion mode (rolling versus sliding) and effectively reflects the fundamental alteration in contact behavior induced by partial wear.

Just Accepted

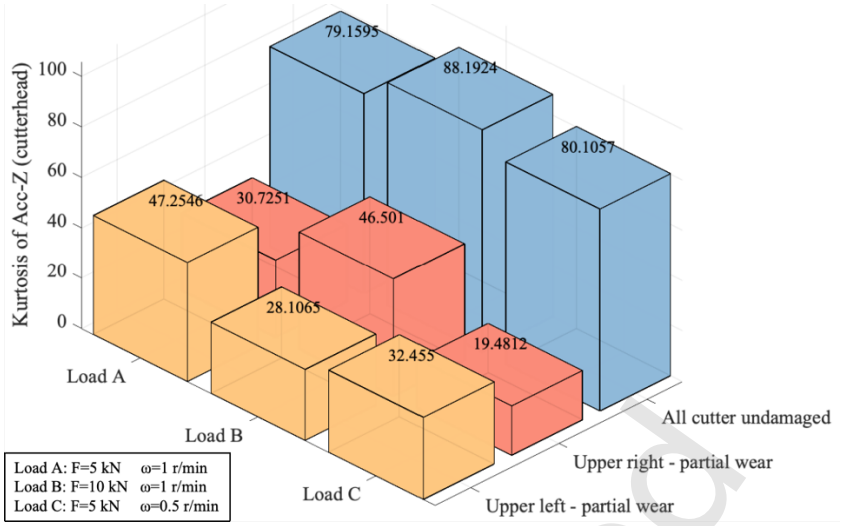


Fig. 9 Kurtosis of the cutterhead

It should be further emphasized that the proposed mechanism of contact mode transition, inferred from the evolution of vibration-based statistical features, is not solely based on signal-level analysis, but is also directly supported by cutter wear morphology observed in previous studies[32]. Existing studies have shown that, during normal rolling penetration, the contact region of the cutter is primarily subjected to normal compressive stress. Accordingly, the cutter ring surface exhibits wear morphology dominated by relatively uniform plastic deformation. Although ploughing grooves may also appear, they are not the dominant feature. In contrast, for partially worn cutters under constrained rotation, the cutter–rock interaction shifts to a sliding-dominated contact mode. As a result, tangential friction and ploughing effects are significantly enhanced, leading to the formation of pronounced directional grooves distributed along the cutting direction at the contact interface (Fig. 10). This transition from rolling to sliding-induced wear mechanisms has been widely recognized as a typical tribological characteristic of partially worn cutters.

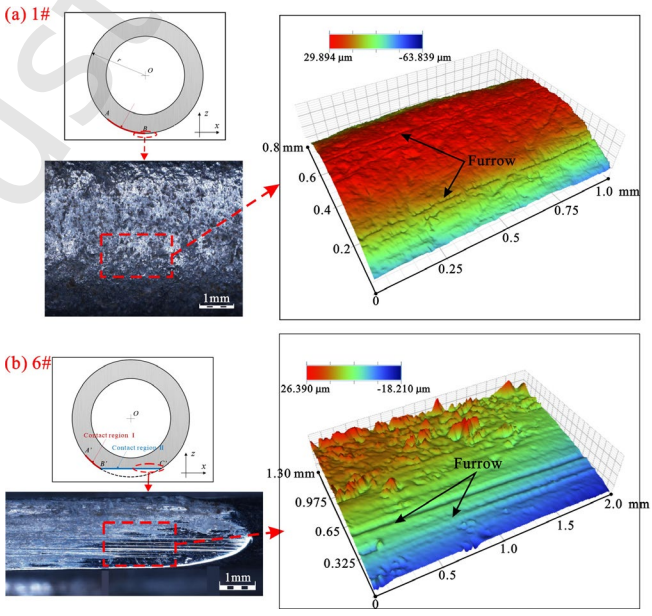


Fig. 10 Microscopic morphology of cutter wear (No. 1: normal wear; No. 6: partial wear)

From the perspective of mechanical response, the load component analysis (Fig. 11) further

Just Accepted

reveals the distinct force characteristics between partially worn cutters and normal cutters. Specifically, the tangential load component of the partially worn cutter increases significantly relative to the normal component, indicating a reduction in normal extrusion effects and a substantial increase in frictional resistance during contact. This change is closely related to both the geometric morphology and motion state of the cutter. Due to the reduced outer profile height and constrained rotation, the cutter is less capable of achieving effective rock breaking through rolling penetration, resulting in insufficient normal compressive force. Meanwhile, the transition to a sliding-dominated contact mode leads to a marked increase in tangential friction and ploughing action, thereby giving rise to higher tangential load components. This mechanical behavior is consistent with the directional ploughing grooves observed in the microscopic morphology (Fig. 10), and is further corroborated by the statistical characteristics of vibration signals, including increased RMS values, significantly elevated cutting coefficient (CC), and reduced kurtosis. Together, these observations demonstrate that the transition of the cutter–rock contact mode—from "rolling indentation" to "sliding scraping"—is a typical physical manifestation associated with partial wear, consistently reflected across mechanical response, surface morphology, and vibration characteristics. This multi-level consistency provides more direct and robust support for the mechanism analysis presented in this study.

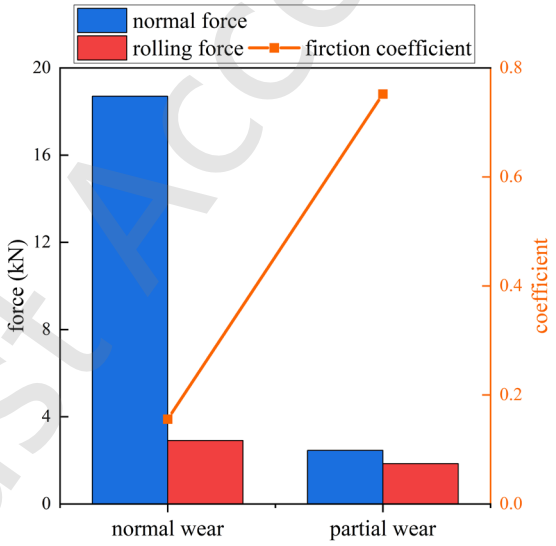


Fig. 11 Variation of cutter load components

Just Accepted

4. Mechanism-Guided State-Conditioned Recognition Framework

Conventional vibration-based state recognition methods typically rely on an implicit assumption: the system state can be determined solely from an instantaneous signal segment. However, TBM cutter damage exhibits a pronounced cumulative-feature characteristic, i.e., the underlying damage state is reflected through statistical signatures that build up over historical interactions. Vibration signals measured within a short time window primarily capture the transient

dynamics of cutter-rock interaction, rather than the intrinsic health state of the cutter itself. Consequently, when the task is formulated as window-level classification, an inherent issue of incomplete state information arises. To address this limitation, this study models the cutter state as a slowly evolving latent damage state over time, rather than a direct function of instantaneous vibration observations. The label of a given time window cannot be uniquely determined by the current observation $x(t)$ alone; instead, it depends on the latent damage state $s(t)$ that evolves over time:

$$y(t) \sim P\left(y \middle| x(t), s(t)\right) \tag{1}$$

where $x(t)$ denotes the instantaneous vibration observation and $s(t)$ denotes the latent damage state of the cutter. Accordingly, the recognition process is decomposed into two complementary components: (1) an observation encoder that characterizes instantaneous vibration patterns; and (2) a mechanism-guided state estimator that captures history-accumulated statistical signatures associated with damage evolution. Based on these components, a state-conditioned recognition framework is constructed, consisting of an observation encoding module, a mechanism-guided state estimation module, and a conditional decision module, as shown in Fig. 12.

In the recognition pipeline illustrated in Fig. 12, a deep neural network is first used to encode multi-channel raw vibration signals and extract instantaneous dynamic-response features. Meanwhile, statistical indicators are constructed from historical vibration sequences based on vibration mechanisms and cutterhead spatial configuration, so as to represent the accumulated effects of cutter-rock interaction. The former describes the observation pattern at the current moment, whereas the latter provides a stable proxy that tracks the evolution of damage-related signatures. Under this formulation, recognition is no longer treated as a plain feature classification problem; instead, it is defined as a state-conditioned inference problem, where instantaneous vibration responses are interpreted and classified under the estimated latent damage state.

The framework follows the principle of learning-deployment consistency: during training, complete sequences are used to obtain stable state estimation to support reliable decision-boundary learning; during testing, only historical information prior to the current window is used for causal state estimation, ensuring that state variables are physically available under online monitoring. In this chapter, Section 4.1 introduces the unified modeling of the observation encoding module; Section 4.2 presents the mechanism-guided state estimation module; and Section 4.3 details the implementation of state-conditioned decision making.

Just Accepted

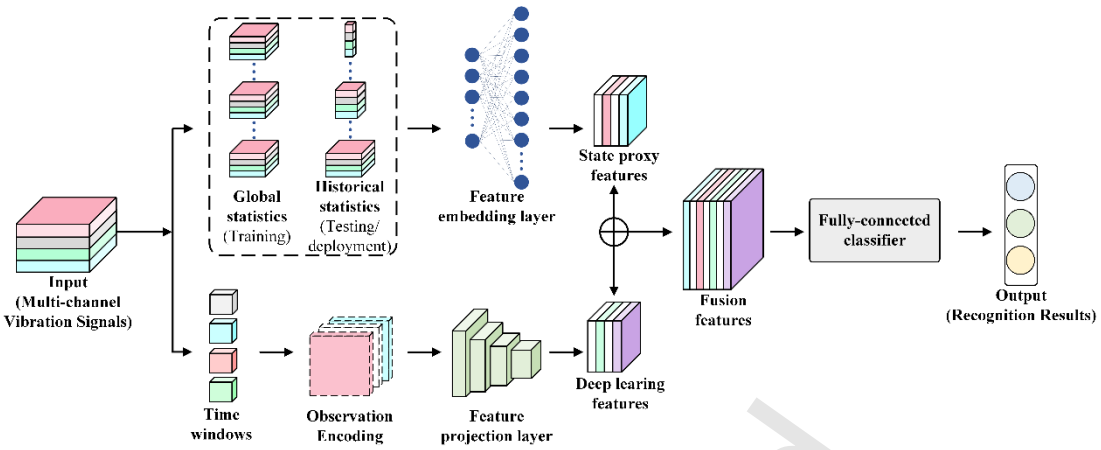


Fig. 12 Proposed state-conditional recognition framework

4.1 Observation Encoding Module

The deep-learning backbone in this study is not directly used to determine the cutter health state. Instead, it serves as an observation encoder that extracts transient dynamic-response features from short-time vibration segments. Notably, this module is not tied to any specific neural architecture; rather, it targets window-level representation learning, providing a unified feature interface for subsequent mechanism-feature fusion and state recognition.

Given a vibration sequence X_i, it is segmented into non-overlapping windows: $X_{i,\omega} \in \mathbb{R}^{C\times L}$, where i denotes the index of the raw signal sample, ω denotes the window index, C is the number of channels, and L is the predefined window length. For each window, a compact representation is learned as:

$$z_t' = f_\theta(X_{i,\omega}) \tag{2}$$

where $f_\theta(\cdot)$ denotes the deep feature extraction function, which can be implemented using different neural networks (e.g., convolution-based architectures or self-attention-based temporal models). This representation captures instantaneous interaction characteristics such as impact responses and local oscillations. Since cutter damage evolves slowly in time, this representation reflects the current observation rather than the latent damage state itself. To provide an architecture-agnostic unified interface, the features are projected into a fixed-dimensional embedding space:

$$z_t = \phi\left(f_\theta(X_{i,\omega})\right) \in \mathbb{R}^D \tag{3}$$

where $\phi(\cdot)$ is a learnable projection function and D denotes the unified embedding dimension.

In summary, this module performs window-level complex temporal pattern modeling only. It outputs a fixed-length representation for each window without cross-window information leakage or decision making. Therefore, it models the instantaneous observation distribution under varying operating conditions rather than the damage state of the cutter. Because this module is open to different backbone designs, two representative deep models are adopted in later experiments to verify the generality and effectiveness of the proposed framework across different modeling

Just Accepted

mechanisms.

4.2 Mechanism-Guided State Estimation Module

In contrast to instantaneous vibration responses, cutter damage is associated with history-dependent physical effects, which manifest in vibration signals mainly as gradually evolving statistical properties rather than abrupt local patterns. Hence, a single time window is insufficient to uniquely determine the cutter state. To obtain background information correlated with the latent damage state, this module constructs physically interpretable statistical indicators from historical vibration signals. These indicators are not used as direct classification features; instead, they serve as state proxies that summarize history-accumulated damage-related signatures:

$$s_t = g(S_{i,\omega}) \tag{4}$$

where $g(\cdot)$ denotes the mechanism-statistical mapping function. Based on the analysis in Chapter 3, $g(\cdot)$ computes dimensionless time-domain statistical indicators that are weakly sensitive to operating conditions but strongly associated with damage-related changes, providing an independent and interpretable information source complementary to deep features. Here, $S_{i,\omega}$ denotes the signal interval used to compute mechanism-guided features. Since these state proxies are derived from historical interactions, global statistics that contain future information are unavailable during testing and real deployment. Therefore, the accessible signal intervals differ between training and testing:

$$S_{i,\omega} = \begin{cases} X_{i,1:T}, & train\ phase \\ X_{i,1:t-1}, & test\ phase \end{cases} \tag{5}$$

Specifically, during training, statistical analysis is performed over the complete sequence of each sample; during testing, a strictly causal strategy is adopted, where mechanism-guided features are computed only from historical data prior to the current window. This design ensures that state proxies are both statistically stable and causally available for online monitoring, preventing "excellent offline performance but degraded field performance" due to information leakage.

A state encoding layer is further introduced to map the state proxy into a learnable state representation:

$$z_{state} = \psi(s_t) \in \mathbb{R}^F \tag{6}$$

where $\psi(\cdot)$ is a learnable embedding function. Its parameters are optimized via backpropagation during training and fixed during testing, ensuring consistent mapping across different signal windows. F denotes the output dimension of the state representation.

With the dual strategy (global statistics for training and causal statistics for testing), the mechanism-guided state estimator satisfies practical deployment constraints while preserving statistical robustness. Moreover, since the state proxies are physically meaningful, their temporal trends can be used to interpret the module output, thereby enhancing the interpretability of the

Just Accepted

overall state recognition framework.

4.3 State-Conditioned Decision

Given the observation representation z_t and the state representation z_{state}, the recognition task is no longer a direct classification problem; instead, it becomes a conditional inference problem. The classifier learns decision boundaries conditioned on the latent damage state:

$$P(y_t \mid x_t, s_t) \tag{7}$$

Since both representations are defined in fixed-dimensional spaces with comparable numerical scales, they can be directly fused via vector concatenation:

$$z = [z_t \parallel z_{state}] \in \mathbb{R}^{D+F} \tag{8}$$

where $\parallel$ denotes vector-level concatenation. This operation avoids mixing or compressing information across feature sources and introduces no additional complex interaction structures. It preserves the integrity of each subspace while achieving a simple and stable fusion in a $D + F$ dimensional feature vector, which is then fed into a linear classifier for state prediction:

$$\hat{y} = Wz + b \tag{9}$$

where $\hat{y}$ denotes the predicted label output by the decision module. Under this formulation, the state representation constrains the interpretation of instantaneous vibration patterns, enabling the classifier to distinguish similar transient responses induced by different latent damage states.

This decision strategy transforms traditional window-level recognition into a state-conditioned decision problem, improving stability and reliability under varying operating conditions while remaining compatible with different deep-learning backbones. It should be noted that the core objective of this study is not to design a sophisticated feature-fusion architecture, but to verify the specific contribution of mechanism-guided state variables to recognition performance. For this reason, a simple concatenation strategy is intentionally adopted, so that the influence of additional fusion modules does not obscure the effect of state conditioning itself.

Overall, the proposed framework retains the end-to-end modeling advantages of deep learning while incorporating interpretable history-dependent information, thereby enhancing recognition accuracy and robustness. During training, the cross-entropy loss is used to jointly optimize all network parameters—including the deep feature extractor, projection layer, mechanism-feature encoder, and classifier—via backpropagation. Because the classifier inherently provides implicit weighting, the framework can automatically learn how to balance the relative contributions of deep features and mechanism-guided features in the fused space without additional manual weighting. By avoiding manually designed fusion weights or complex interaction structures, the framework preserves architectural simplicity and ensures that the observed improvements stem from the mechanism-guided conditioning strategy rather than from fusion techniques.

Just Accepted

5. Results and Discussion

5.1 Experimental Environment and Settings

The experiments in this study were conducted in an environment configured with PyTorch 2.5.1, Python 3.12, and CUDA 12.4. The computational platform was equipped with an NVIDIA RTX 3090 GPU (24 GB VRAM), a 14-core Intel Xeon Platinum 8362 @2.80 GHz CPU, and 45 GB of RAM.

The experimental data were obtained from the TBM cutter rock-breaking tests under multiple operating conditions introduced in Chapter 2. Each dataset lasted 180 s and was standardized using z-score normalization and associated with explicit state labels. Each 180 s dataset was acquired from a single, independent, and continuous experimental run. Considering the inherently stochastic and non-stationary nature of the cutter-rock interaction process, repeated experiments under the same operating condition were not conducted. To evaluate the generalization performance of the proposed recognition framework under varying operating conditions, a cross-condition train-test strategy was adopted: the model was trained on the dataset collected under one operating condition and tested on another, forming a typical cross-condition task (e.g., A → B). The definitions of working-condition labels and damage-state labels are summarized in Table 1 and Table 2, respectively.

It should be noted that force sensors in the experimental setup were primarily used for monitoring and controlling operating conditions, rather than for constructing the learning dataset. Considering that lateral acceleration components of the cutter typically exhibit limited diagnostic relevance in this context, only the rolling-direction and normal-direction acceleration signals were selected. Specifically, two sensors were used, and their rolling and normal components (four channels in total) were employed to construct the input dataset.

Table 1 Definition of working-condition labels

Label	Definition
A	F=5 kN， ω=1 r/min
B	F=10 kN， ω=1 r/min
C	F=5 kN， ω=0.5 r/min

Table 2 Definition of damage-state labels

Label	Definition
0	All cutter undamaged
1	Upper right - partial wear
2	Upper left - partial wear

Following the data processing procedure described in Chapter 4, raw vibration signals were segmented into non-overlapping windows with a window length of 512 time steps, corresponding to a window duration of approximately 0.1024 s. Each window was treated as an independent sample for prediction and decision-making. For each working-condition dataset, 1757 labeled window

Just Accepted

samples were obtained. All samples participated in training or testing, while strict window-level separation between the training set and the test set was maintained. For example, in a single run, all 1757 window samples from Condition A were used for training (including internal validation during backpropagation), and all 1757 samples from Condition B were used as the test set to evaluate cross-condition generalization. As a result, the training and testing windows are drawn from different experimental runs rather than from the same continuous signal, effectively avoiding potential information leakage caused by shared data sources. To reduce randomness, repeated experiments were conducted: 10 independent runs were performed, and the mean recognition accuracy and its standard deviation were reported as the final performance metrics.

To verify the adaptability of the proposed fusion framework to different deep learning modeling mechanisms, two representative deep models were selected as backbone feature extractors: (1) DCNN, built upon convolutional structures, emphasizing discriminative feature extraction from local time-domain and frequency-domain patterns; (2) Transformer, built upon self-attention mechanisms, enabling modeling of long-range dependencies within each window. Under the unified experimental setup, both backbones followed the state-conditioned decision strategy proposed in Chapter 4: after introducing the mechanism-guided state variables, the two representations were concatenated for final cutter state recognition.

For each dataset, the mechanism-guided state variables are derived differently in the training and testing phases. During training, they are computed from the complete dataset, resulting in identical state variable values for all windows within that dataset. During testing, however, the state variables are updated recursively using only the historical data available prior to the current window, thereby preserving temporal causality. In this work, each state variable is defined by an explicit mathematical equation computed from designated sensor channels, the specific equations are as follows:

$$\rho_{r,n}^{cutter} = \frac{\sum_{i=1}^{N}\left(a_{r,cutter,i} - \overline{a_{r,cutter}}\right)\left(a_{n,cutter,i} - \overline{a_{n,cutter}}\right)}{\sqrt{\sum_{i=1}^{N}\left(a_{r,cutter,i} - \overline{a_{r,cutter}}\right)^2}\sqrt{\sum_{i=1}^{N}\left(a_{n,cutter,i} - \overline{a_{n,cutter}}\right)^2}} \tag{10}$$

$$Ratio_{RMS}^{cutter} = \frac{\sqrt{\frac{1}{N}\sum_{i=1}^{N} a_{r,cutter,i}^2}}{\sqrt{\frac{1}{N}\sum_{i=1}^{N} a_{n,cutter,i}^2}} \tag{11}$$

$$Ratio_{RMS}^{cutterhead/cutter} = \frac{\sqrt{\frac{1}{N}\sum_{i=1}^{N} a_{r,cutterhead,i}^2 + a_{n,cutterhead,i}^2}}{\sqrt{\frac{1}{N}\sum_{i=1}^{N} a_{r,cutter,i}^2 + a_{n,cutter,i}^2}} \tag{12}$$

Just Accepted

$$Kurtosis_r^{cutterhead} = \frac{\frac{1}{N}\sum_{i=1}^{N}\left(a_{r,cutterhead,i} - \overline{a_{r,cutterhead}}\right)^4}{\left(\frac{1}{N}\sum_{i=1}^{N}\left(a_{r,cutterhead,i} - \overline{a_{r,cutterhead}}\right)^2\right)^2} \tag{13}$$

$$Kurtosis_n^{cutterhead} = \frac{\frac{1}{N}\sum_{i=1}^{N}\left(a_{n,cutterhead,i} - \overline{a_{n,cutterhead}}\right)^4}{\left(\frac{1}{N}\sum_{i=1}^{N}\left(a_{n,cutterhead,i} - \overline{a_{n,cutterhead}}\right)^2\right)^2} \tag{14}$$

where $a_{r,cutter,i}$ and $a_{n,cutter,i}$ denote the rolling-direction and normal-direction acceleration of the cutter at the *i*-th sampling point, respectively. $a_{r,cutterhead,i}$ and $a_{n,cutterhead,i}$ represent the corresponding rolling and normal acceleration components measured on the cutterhead. $\overline{a_{(\cdot)}}$ denotes the mean value of the corresponding signal.

The two models employed the same fusion-layer design. Specifically, window-level deep features produced by the backbone were projected to a unified dimension $D = 128$ through a feature projection layer. Mechanism-guided statistical features were mapped into an embedding of dimension $F = 64$. The final fused feature vector had dimension $D + F = 192$.

During training, the cross-entropy loss was used as the optimization objective, and parameters were updated using the Adam optimizer. Table 3 and Table 4 list the key hyperparameters of the backbone models and the training settings, respectively. These parameters were selected through preliminary experiments to ensure sufficient representational capacity while avoiding excessive model complexity. The training settings also yielded stable optimization behavior, where the loss decreased rapidly at early epochs and gradually converged. Unless explicitly stated (e.g., setting the state variable inputs to zero for comparison), all parameter settings were kept identical across experiments.

Table 3 Hyperparameters of backbone models

Model	Parameter	Value
DCNN	Input channels	4
	Feature dimension	16
	Conv1 kernel size	(32, 3)
	Conv2 kernel size	(16, 1)
Transformer	Model dimension	64
	Attention heads	4
	Number of encoder layers	3
	Feed-forward dimension	256

Table 4 Training parameter settings

Parameter	Value
Batch size	128
Training epochs	30 (DCNN) / 20 (Transformer)

Just Accepted

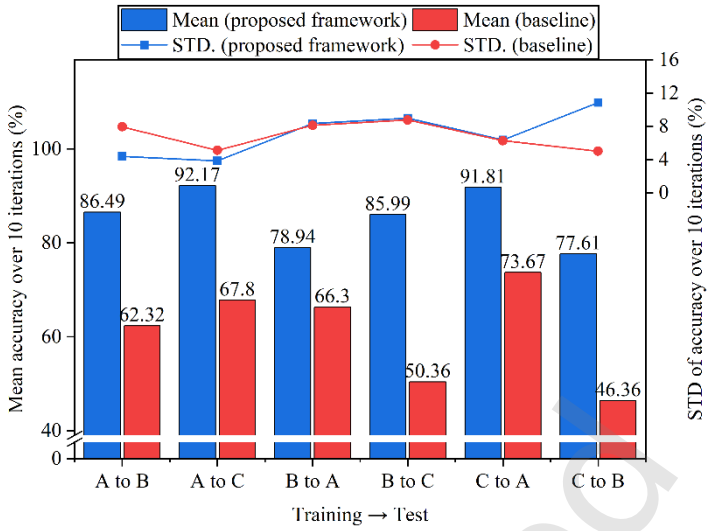
Learning rate	1e-4 (DCNN) / 2e-4 (Transformer)
Dropout rate	0.1
Repeated iterations	10

5.2 Validation of Cross-Condition Stability

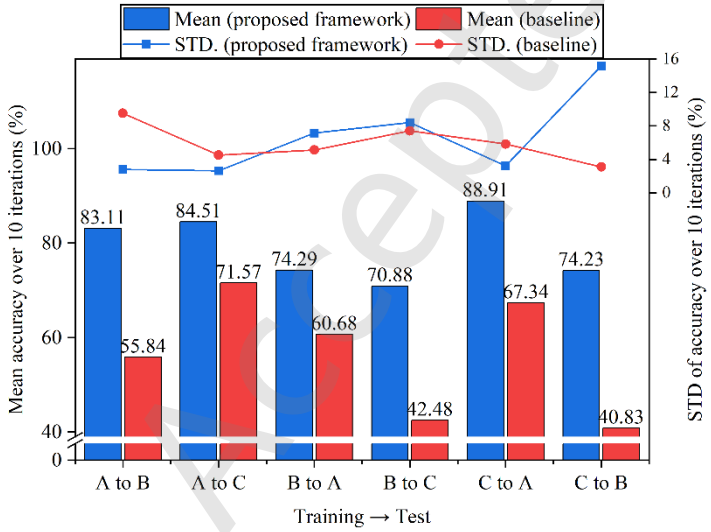
To validate the decision stability of the proposed mechanism-guided state-conditioned recognition framework under complex varying operating conditions, cross-condition experiments were conducted. The key question is whether the model can continuously produce consistent cutter state predictions when external operating conditions change, rather than misinterpreting condition differences as state differences. Conventional deep models relying only on window-level instantaneous vibration observations mainly base their decisions on the statistical distribution and local waveform patterns within the current window. When thrust, rotational speed, and other working-condition change, the vibration distribution often undergoes substantial drift, leading to condition-dependent shifts of the decision boundary and a significant degradation of cross-condition performance. By introducing a mechanism-guided state variable constructed from historical statistics as a state-conditioned constraint, the proposed framework aims to reduce observation ambiguity and suppress the interference of working-condition perturbations on the decision boundary, thereby improving stability and robustness under cross-condition scenarios.

Fig. 13 summarizes the recognition accuracy (mean ± standard deviation over 10 runs) obtained with DCNN and Transformer as the observation encoding module across different train-test working-condition pairs. The results show that for all cross-condition tasks, the complete framework with the mechanism-guided state variable achieves higher and more stable performance. The best accuracy reaches 92.17% (DCNN) and 88.91% (Transformer). Compared with the instantaneous-observation-only classifier (baseline), accuracy is consistently improved across tasks. These results indicate that mechanism-guided state information effectively mitigates distribution shifts induced by varying operating conditions, encouraging the classifier to focus on decision evidence related to cutter state rather than spurious patterns correlated with a specific condition. Moreover, both backbones exhibit consistent performance gains despite their distinct modeling mechanisms, further validating the backbone-agnostic nature and architectural generality of the proposed framework.

Just Accepted



(a) DCNN

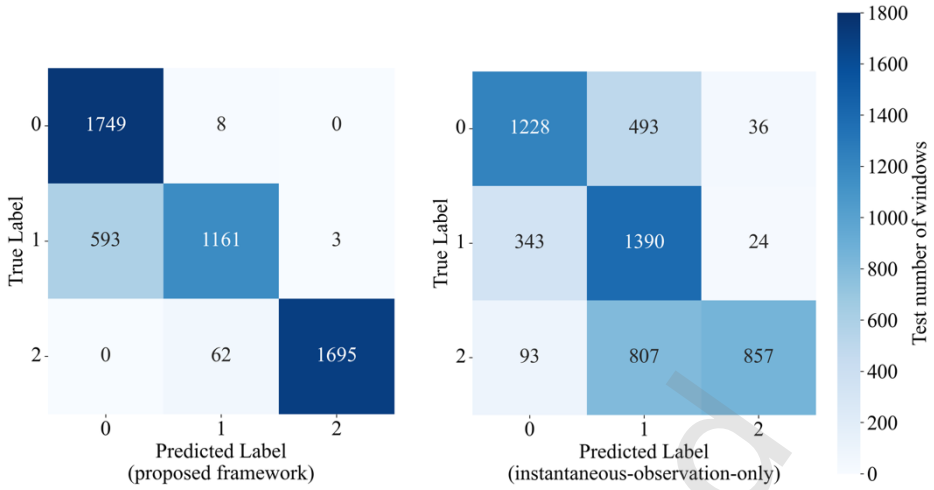


(b) Transformer

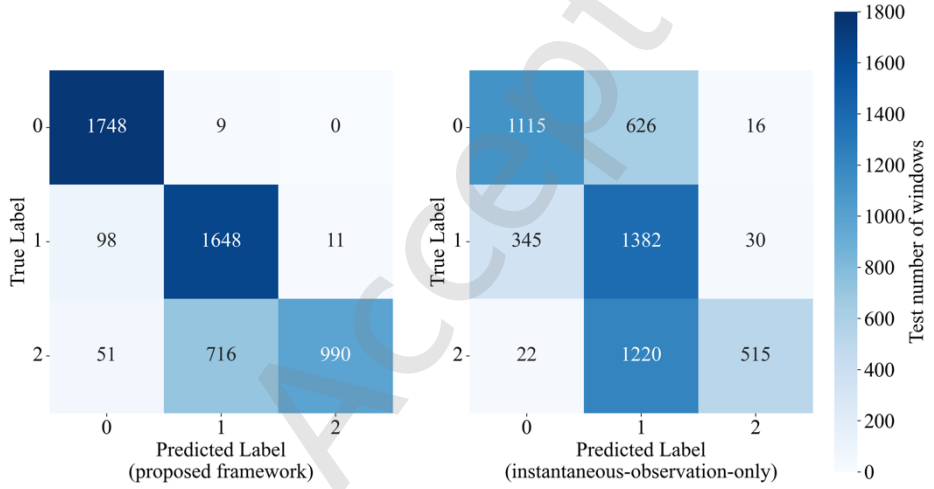
Fig. 13 Cross-condition recognition accuracy under different working-condition pairs

To visualize state confusion, Fig. 14 compares the confusion matrices of a representative task (train on Condition A → test on Condition B) between the complete framework (left) and the instantaneous-observation-only classifier (right). The complete framework significantly reduces misclassification across all classes, particularly alleviating confusion between classes that are sensitive to working-condition perturbations. This demonstrates that the state-conditioned constraint provided by the state estimation module restricts the interpretation space of instantaneous vibration patterns, shifting the decision boundary from being “condition-sensitive” to being “state-sensitive”, thereby improving cross-condition consistency.

Just Accepted



(a) DCNN

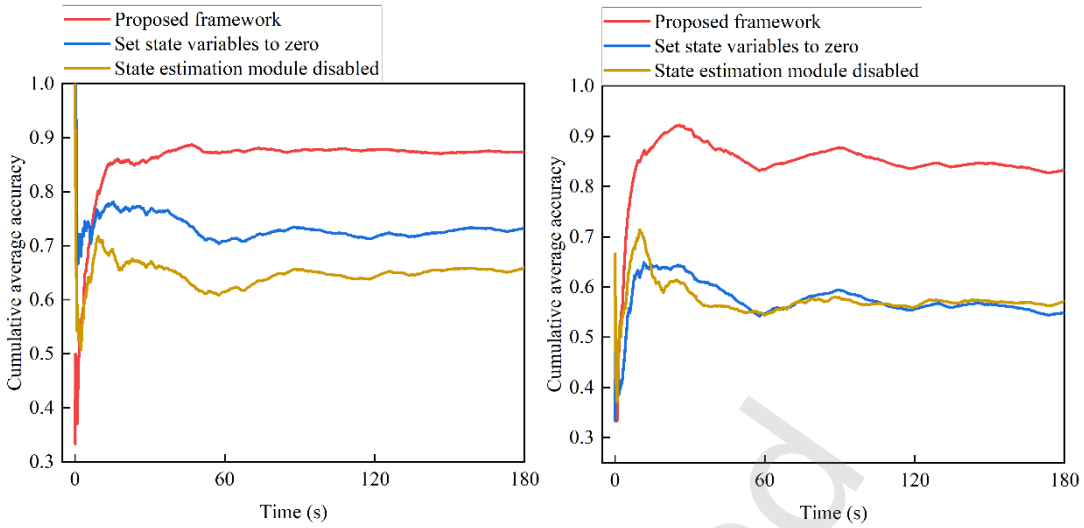


(b) Transformer

Fig. 14 Confusion matrices for the A→B task

Because the mechanism-guided state variable in the testing phase is computed from historical statistics, its estimation quality improves progressively as more history becomes available. Consequently, the decision performance of the framework exhibits a dynamic convergence process. Fig. 15 shows the time-cumulative average accuracy curves for the representative A → B task, comparing the complete framework with a variant where the state estimation module is disabled (or its outputs are set to zero). With state conditioning, the overall accuracy increases substantially and gradually stabilizes. At the early stage of monitoring, the complete framework may exhibit some state uncertainty due to limited historical information. As the statistical horizon expands over time, the constraint imposed by the state estimator becomes stronger, enabling the model to continuously correct early uncertainties and converge to stable performance.

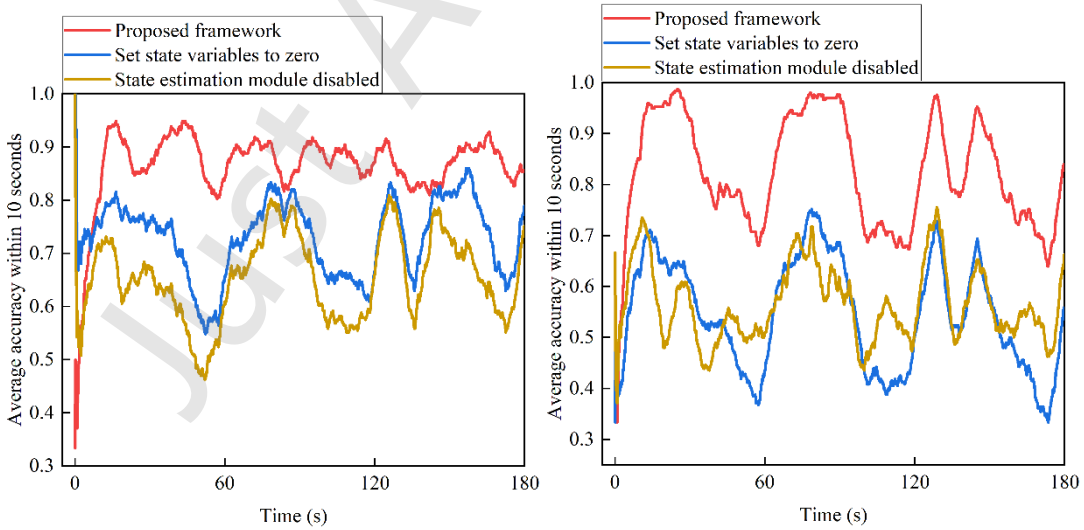
Just Accepted



(a) DCNN (b) Transformer

Fig. 15 Time-cumulative average accuracy curves for the A→B task

To further analyze recognition performance under short observation horizons, Fig. 16 reports the average accuracy within the 10s of testing time. When relying only on instantaneous observations (disabling the state estimation module or setting all its outputs to zero), performance is more sensitive to working-condition changes and shows pronounced fluctuations. In contrast, after introducing the mechanism-guided state conditioning, accuracy improves across all time intervals and variability is substantially reduced. This indicates that the state variables formed by historical statistics effectively reduce observation uncertainty caused by working-condition variations, thereby improving the reliability of short-horizon recognition.



(a) DCNN (b) Transformer

Fig. 16 Average accuracy within the 10s for the A→B task

To further verify that the performance gain arises from state-conditioned modeling rather than a potential privileged-statistics effect during training, additional experiments were conducted using DCNN on the A→B task with 10 repeated iterations. Three statistical settings were considered: (i) global training/causal testing (proposed method), (ii) causal training/causal testing (lower-bound

Just Accepted

reference), and (iii) global training/global testing (upper-bound reference). Here, “global” indicates that state variables are computed from the complete dataset, whereas “causal” denotes recursive estimation using only historical data prior to the current time step.

The results show that (in Fig. 17), compared with the causal training/causal testing setting, the proposed global training/causal testing strategy achieves significantly better performance, indicating that global statistics during training help establish clearer state-discriminative boundaries. Moreover, the performance remains close to the upper bound (global training/global testing) under strict causal constraints, demonstrating that the improvement does not stem from future information leakage but from the effective constraint imposed by mechanism-guided state variables.

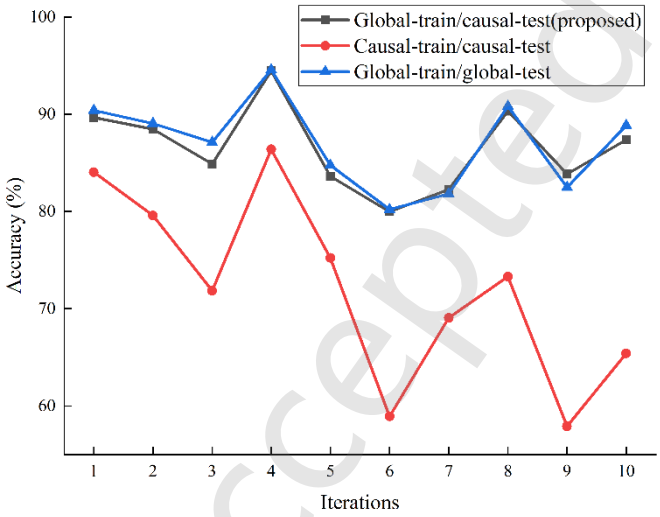


Fig. 17 Statistical-strategy comparison with 10 repeated iterations

Overall, the cross-condition accuracy results, confusion-matrix comparisons, time-evolution analyses, and the statistical-strategy comparison experiments consistently demonstrate that the proposed framework maintains stable cutter state recognition under varying operating conditions, significantly suppressing decision-boundary perturbations induced by working-condition changes, and improving temporal stability.

5.3 Ablation Study (DCNN, Condition A → Condition B)

To further quantify the contribution of the mechanism-guided state variables to cross-condition cutter state recognition, an ablation study was conducted on the A → B task using DCNN as the observation encoding module. By progressively removing or retaining different categories of mechanism-guided statistical information, the effect of each type of state proxy on recognition performance was evaluated, thereby validating the effectiveness of state-conditioned modeling. Notably, when all state variables are removed, the framework degenerates into a conventional window-level classifier purely driven by instantaneous vibration observations.

According to the mechanism analysis in Chapter 3 and the state estimation design in Section 4.2, the mechanism-guided state variables used in this study can be grouped into three categories: (1) Correlation: correlation-related indicators between horizontal and vertical vibrations; (2) Kurtosis: impact-sensitive statistical indicators; (3)RMS Ratio: energy-distribution ratio indicators.

Just Accepted

Based on the complete framework, three ablation settings were designed: (i) Remove one category, to assess its marginal contribution; (ii) Keep only one category, to test the sufficiency of a single state proxy; (iii) Remove all categories, to evaluate performance degradation without state conditioning. All experiments were repeated 10 times, and mean recognition accuracy was reported. The results are shown in Fig. 18.

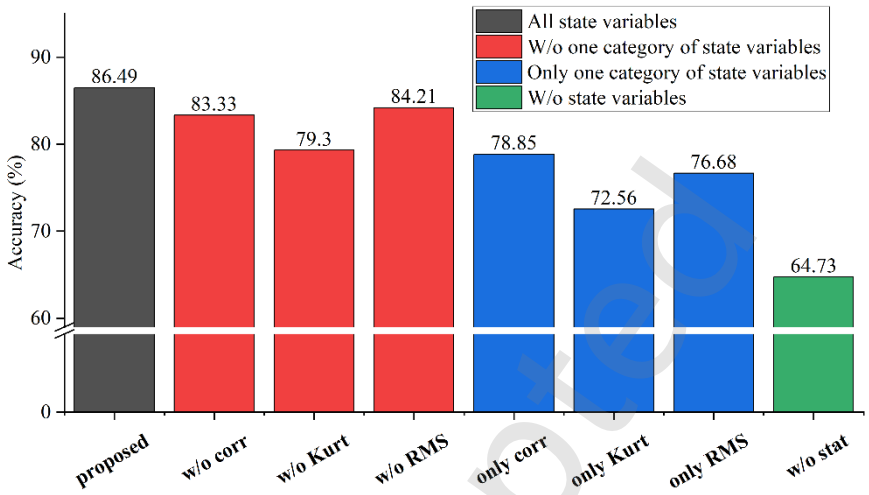


Fig. 18 Ablation study results

With all state variables included, the framework achieves the highest accuracy of 86.49%. Removing any single category leads to performance degradation: removing Correlation reduces accuracy to 83.33%; removing Kurtosis reduces accuracy to 79.30%; removing RMS Ratio reduces accuracy to 84.21%. Among these, removing Kurtosis results in the most pronounced degradation, indicating that changes in impact sparsity and amplitude distribution are more strongly associated with cutter state evolution and provide more effective constraints for cross-condition decision making. Correlation and RMS Ratio still provide stable complementary contributions, suggesting that different mechanism-guided statistics offer non-redundant gains.

The “keep only one category” results further show that a single type of state proxy is insufficient for robust cross-condition recognition: keeping only Correlation yields 78.85%, keeping only Kurtosis yields 72.56%, and keeping only RMS Ratio yields 76.68%. All are notably lower than the complete model, indicating that statistical signatures of cutter state are intrinsically multi-dimensional. A single state variable cannot resolve all observation ambiguities under varying operating conditions, whereas multiple categories provide complementary constraints that form a more stable state-conditioned representation.

When all mechanism-guided state variables are removed, accuracy drops sharply to 64.73%. In this case, the classifier relies entirely on instantaneous observations, making its decision boundary highly susceptible to distribution drift induced by changes in operating conditions, and thus prone to misinterpreting working-condition differences as state differences. This result demonstrates that the role of mechanism-guided state variables is not merely to “add extra features”, but to provide state-conditioned information reflecting history-dependent evolution, constraining the interpretation of instantaneous observations and shifting the model from “instantaneous-observation-driven” to

Just Accepted

"stable decision under state-conditioned constraints".

Overall, the ablation study reveals a continuous degradation trend as state variables are progressively removed, suggesting that performance gains mainly arise from effective supplementation of state information via mechanism-guided historical statistics, rather than incidental benefits from increased structural complexity. This conclusion aligns with the cross-condition stability results in Section 5.2 and further supports the effectiveness and engineering potential of the proposed state-conditioned recognition framework under complex varying operating conditions.

5.4 Discussion

This chapter systematically evaluated the proposed mechanism-guided state-conditioned recognition framework under cross-condition scenarios. Compared with conventional deep learning models that rely only on instantaneous window observations, the proposed framework exhibits a more stable decision boundary when operating conditions change. This indicates that purely observation-driven learning is vulnerable to vibration distribution drift, whereas state-conditioned constraints provide additional structural information in the feature space, thereby reducing observation ambiguity caused by varying operating conditions.

The time-evolution analysis further reveals the operational mechanism of the state variables in the recognition process. Since mechanism-guided features are computed using historical statistics during testing, their values become progressively more stable as the historical horizon accumulates, leading to a characteristic transition from early-stage fluctuations to later-stage convergence in recognition performance. This suggests that the state estimation module fundamentally provides time-scale complementary information for instantaneous vibration patterns, rather than simply appending extra features.

The ablation study clarifies the functional roles of different mechanism-guided state variables. Impact statistics (Kurtosis) show a strong influence on recognition performance, reflecting the direct impact of cutter motion-mode changes on the vibration distribution. Correlation and RMS Ratio provide additional structural constraints. As state variables are gradually removed, performance degrades continuously, indicating that the performance improvement stems from the constraint effect of state information on the decision boundary, rather than changes in network capacity.

Overall, these experimental results demonstrate that separately modeling state proxies derived from historical statistics and instantaneous observation features can effectively suppress cross-condition distribution shifts and improve temporal stability of cutter state recognition.

6 Conclusion

Based on a scaled multi-cutter rock-breaking experimental platform, this study conducted bench tests to address the long-standing challenge of stable recognition of partially worn TBM cutter under complex and varying operating conditions. By integrating the experimental findings with

Just Accepted

deep-learning based modeling, we proposed a mechanism-guided state-conditioned recognition framework and evaluated its recognition performance through systematic cross-condition experiments. The main conclusions are summarized as follows.

1. The multi-cutter cooperative rock-breaking experiments and the corresponding vibration mechanism analysis indicate that TBM cutter rock breaking is essentially dominated by random impacts induced by discontinuous brittle fracture of the rock. Consequently, vibration responses exhibit strong non-stationarity and broadband stochastic characteristics, making it difficult to form stable fault characteristic frequencies. The experimental results further reveal that partial wear does not merely change vibration amplitude, but instead drives a transition of the cutter-rock contact mode from rolling indentation to sliding scraping, thereby reshaping the system's energy distribution and impact-related statistical properties. Motivated by this mechanism, statistical indicators such as the Cutting Coefficient (CC), Kurtosis, and vibration-energy ratio metrics can effectively reflect changes in cutter motion mode and contact behavior, providing a physically meaningful basis for describing the cumulative-feature characteristics of cutter damage states.

2. To overcome the limitation of conventional window-level recognition methods that rely solely on instantaneous observations and fail to capture long-term state regularities, this study models the cutter state as a time-evolving latent variable and constructs a state-conditioned recognition framework consisting of an observation encoding module and a state estimation module. By separately modeling instantaneous vibration responses and state-related information derived from historical statistics, the recognition task is reformulated from direct classification into state-conditioned inference, enabling the framework to interpret current observations under an estimated damage-state context. Moreover, by adopting global statistics during training and historical statistics during testing, the framework ensures consistency between learning and practical online monitoring, effectively avoiding future-information leakage.

3. Cross-condition recognition and ablation results demonstrate that, after introducing mechanism-guided state variables, different deep-learning backbones (DCNN and Transformer) exhibit consistent performance improvements, and the sensitivity to vibration distribution shift caused by varying operating conditions is significantly reduced. Time-evolution analysis further shows that, as historical statistics accumulate progressively, the recognition output transitions from early-stage uncertainty to stable decision-making, indicating that state-conditioned modeling effectively enhances temporal consistency and cross-condition stability. Ablation studies also confirm that different mechanism-guided statistics play complementary roles in state representation, and that the observed performance gains originate from the state-information constraint mechanism rather than increased network complexity.

It should be emphasized that this study is conducted within a deliberately controlled experimental scope. All experiments are performed on a scaled multi-cutter rock-breaking platform using a single lithology (granite) and a fixed pre-machined partial wear depth of 2 mm, while complex mechanical coupling among cutters is intentionally simplified. This design allows the

Just Accepted

causal relationship between local cutter wear, contact-mode transition, and vibration statistical responses to be examined in a clear and reproducible manner. At the same time, it implies that the present work does not establish quantitative relationships across different wear severities, lithologies, or strongly coupled multi-cutter environments. Moreover, the validation relies solely on laboratory bench data, and the comparative analysis is intentionally confined to deep-learning models with and without state conditioning in order to isolate the specific contribution of the mechanism-guided state variables. Therefore, the conclusions should be interpreted as a verification of the proposed mechanism and methodology under controlled experimental conditions. Future work will extend the investigation to multi-lithology and progressive-wear scenarios, and will incorporate long-term monitoring data from real TBM operations together with broader comparisons involving various fault diagnosis approaches and transfer learning strategies to further assess the advantages of the proposed framework.

Acknowledgements

This work was supported by the National Natural Science Foundation of China (No. 52475218 and 52405220), Fundamental Research Funds for the Central Universities (No. 2682024CG008).

Just Accepted

Reference

[1] HYUN K-C, MIN S, CHOI H, et al. Risk analysis using fault-tree analysis (FTA) and analytic hierarchy process (AHP) applicable to shield TBM tunnels [J]. Tunnelling and Underground Space Technology, 2015, 49: 121-9.

[2] AGRAWAL A K, MURTHY V M S R, CHATTOPADHYAYA S. Investigations into reliability, maintainability and availability of tunnel boring machine operating in mixed ground condition using Markov chains [J]. Engineering Failure Analysis, 2019, 105: 477-89.

[3] FARROKH E, KIM D Y. A discussion on hard rock TBM cutter wear and cutterhead intervention interval length evaluation [J]. Tunnelling and Underground Space Technology, 2018, 81: 336-57.

[4] SU W, LI X, JIN D, et al. Analysis and prediction of TBM disc cutter wear when tunneling in hard rock strata: A case study of a metro tunnel excavation in Shenzhen, China [J]. Wear, 2020, 446-447.

[5] WANG S, ZHANG M, MO J. On the contact and vibration characteristics of TBM cutter with abnormal damage under hard rock conditions [J]. Wear, 2025, 562-563.

[6] LI Y, SCHREIBER P, SCHNEIDER J, GREINER C. Tribological mechanisms of slurry abrasive wear [J]. Friction, 2022, 11(6): 1079-93.

[7] SHANKAR V K, KUNAR B M, MURTHY C S, RAMESH M R. Measurement of bit-rock interface temperature and wear rate of the tungsten carbide drill bit during rotary drilling [J]. Friction, 2020, 8(6): 1073-82.

[8] AKHLAGHI M A, BAGHERPOUR R, HOSEINIE S H. Real-time monitoring of disc cutter wear in tunnel boring machines: A sound and vibration sensor-based approach with machine learning technique [J]. Journal of Rock Mechanics and Geotechnical Engineering, 2025, 17(3): 1700-22.

[9] SHIN Y J, KWON K, BAE A, et al. Machine learning-based prediction model for disc cutter life in TBM

excavation through hard rock formations [J]. Tunnelling and Underground Space Technology, 2024, 150.
[10] ZHANG N, SHEN S-L, ZHOU A, CHEN X. Identification of cutter flat wear for rock TBMs using vibration signal of shield [J]. Mechanical Systems and Signal Processing, 2025, 223.
[11] YI S, LI J, LIU Y, et al. In-situ formation of tribofilm with Ti3C2Tx MXene nanoflakes triggers macroscale superlubricity [J]. Tribology International, 2021, 154.
[12] YI S, CHEN X, LI J, et al. Macroscale superlubricity of Si-doped diamond-like carbon film enabled by graphene oxide as additives [J]. Carbon, 2021, 176: 358-66.
[13] YI S, GUO Y, LI J, et al. Two-dimensional molybdenum carbide (MXene) as an efficient nanoadditive for achieving superlubricity under ultrahigh pressure [J]. Friction, 2022, 11(3): 369-82.
[14] YI S, LI J, ZHU J, et al. Investigation of machining Ti-6Al-4V with graphene oxide nanofluids: Tool wear, cutting forces and cutting vibration [J]. Journal of Manufacturing Processes, 2020, 49: 35-49.
[15] LIU M, LIAO S, YANG Y, et al. Tunnel boring machine vibration-based deep learning for the ground identification of working faces [J]. Journal of Rock Mechanics and Geotechnical Engineering, 2021, 13(6): 1340-57.
[16] MO D, BAI L, HUANG W, et al. TBM disc cutter wear prediction using stratal slicing and IPSO-LSTM in mixed weathered granite stratum [J]. Tunnelling and Underground Space Technology, 2024, 148.
[17] KWON K, CHOI H, JUNG J, et al. Prediction of abnormal TBM disc cutter wear in mixed ground condition using interpretable machine learning with data augmentation [J]. Journal of Rock Mechanics and Geotechnical Engineering, 2025, 17(4): 2059-71.
[18] LI L, TAO J-F, YU H-D, et al. Online Condition Monitoring of Gripper Cylinder in TBM Based on EMD Method [J]. Chinese Journal of Mechanical Engineering, 2017, 30(6): 1325-37.
[19] MAHMOODZADEH A, MOHAMMADI M, HASHIM IBRAHIM H, et al. Machine learning forecasting models of disc cutters life of tunnel boring machine [J]. Automation in Construction, 2021, 128.
[20] ZHOU P, LIU C, XU J, et al. SSFLNet: A Novel Fault Diagnosis Method for Double Shield TBM Tool System [J]. Sensors (Basel), 2024, 24(8).
[21] CHEN Z, GRYLLIAS K, LI W. Mechanical fault diagnosis using Convolutional Neural Networks and Extreme Learning Machine [J]. Mechanical Systems and Signal Processing, 2019, 133.
[22] JIANG F, KUANG Y, LI T, et al. Towards Enhanced Interpretability: A Mechanism-Driven domain adaptation model for bearing fault diagnosis across operating conditions [J]. Mechanical Systems and Signal Processing, 2025, 225.
[23] XIANG L, BING H, LI X, HU A. A frequency channel-attention based vision Transformer method for bearing fault identification across different working conditions [J]. Expert Systems with Applications, 2025, 262.
[24] ZHAO R, YAN R, CHEN Z, et al. Deep learning and its applications to machine health monitoring [J]. Mechanical Systems and Signal Processing, 2019, 115: 213-37.
[25] SHEN S, LU H, SADOUGHI M, et al. A physics-informed deep learning approach for bearing fault detection [J]. Engineering Applications of Artificial Intelligence, 2021, 103.
[26] LIU J, CAO H, DHUPIA J S, et al. An adaptive source-free unsupervised domain adaptation method for mechanical fault detection [J]. Mechanical Systems and Signal Processing, 2025, 228.
[27] JIA N, HUANG W, DING C, et al. Physics-informed unsupervised domain adaptation framework for cross-machine bearing fault diagnosis [J]. Advanced Engineering Informatics, 2024, 62.
[28] XIAO Q, YANG M, YAN J, SHI W. Feature decoupling integrated domain generalization network for bearing fault diagnosis under unknown operating conditions [J]. Sci Rep, 2024, 14(1): 30848.
[29] KIM S, SEO Y-H, PARK J. Transformer-based novel framework for remaining useful life prediction of lubricant in operational rolling bearings [J]. Reliability Engineering & System Safety, 2024, 251.
[30] WANG S, ZHANG M, MO J. Contact-Vibration characteristics of TBM cutters with abnormal wear under
Just Accepted

multiple cutter and composite formation conditions [J]. Tunnelling and Underground Space Technology, 2026, 167.
[31] SUN R, ZHANG M, MO J, et al. Coupling effect of cross-section and contact status on load and vibration characteristics of TBM cutters [J]. Mechanical Systems and Signal Processing, 2025, 224.
[32] SUN R, MO J, ZHANG M, et al. Cutting performance and contact behavior of partial-wear TBM disc cutters: A laboratory scale investigation [J]. Engineering Failure Analysis, 2022, 137.



Jiliang Mo (the first author). He received his Ph.D. degree in mechanical design and theory from Southwest Jiaotong University, China, in 2008. His current position is a Professor with Southwest Jiaotong University. His research interests include tribology/dynamic behavior analysis, vibration and noise control, fault diagnosis and intelligence, as well as embodied intelligent robotics. In recent years, he has published more than 200 academic papers in both Chinese and English journals.



Mengqi Zhang (the corresponding author). He received his Ph.D. degree in mechanical design and theory from Northwestern Polytechnical University, China, in 2019. He is currently an Associate Research Fellow with Southwest Jiaotong University, China. His research interests include tribology, contact mechanics, numerical methods, mechanical rock-breaking theory and applications, as well as deep-learning-based fault monitoring methods. In recent years, he has published more than 40 academic papers.



Shengxin Wang (the second author). He is currently pursuing the Ph.D. degree in mechanical design and theory at Southwest Jiaotong University, China. His research interests mainly include self-powered and vibration energy harvesting technologies, damage mechanisms and contact-vibration behavior of heavy-duty friction components in rail transit systems, as well as intelligent diagnosis methods integrating deep learning and mechanism models.



Zhang Zhiyao (the third author). She received the Ph.D. degree in management science and engineering from Chongqing University, China, in 2023. She is currently an Assistant Professor with the Southwest Jiaotong University, China. Her research interests include health prediction and fault diagnosis of complex equipment, tribology, and dynamic analysis.

Just Accepted